Perturbation-assisted Observation of the Lowest Vibrational Level of the $b^3\Pi_0$ State of Ultracold LiK Molecules

Anbang Yang,^{1,*} Xiaoyu Nie,^{1,*} Hao Lin Yu,¹ Yiming Liu,¹ Victor Avalos,¹ Canming He,² Jacek Klos,³ Svetlana Kotochigova,³ and Kai Dieckmann^{1,2,†}

¹Centre for Quantum Technologies (CQT), 3 Science Drive 2, Singapore 117543 ²Department of Physics, National University of Singapore, 2 Science Drive 3, Singapore 117542 ³Department of Physics, Temple University, Philadelphia, PA, 19122, USA (Dated: October 22, 2025)

The narrow transition from the lowest rovibrational level of the $X^1\Sigma^+$ electronic ground state to the lowest vibrational level of the $b^3\Pi_0$ potential provides opportunities for achieving magic-wavelength trapping of ultracold bialkali molecules for enhancing their rotational coherence times. Guided by existing spectroscopic data of several perturbed and deeply-bound rovibrational states of the $A^1\Sigma^+$ potential [Grochola et al., *Chem. Phys. Lett.*, 2012, **535**, 17-20], we conducted a targeted spectroscopic search and report the first observation of the lowest vibrational level of the $b^3\Pi_0$ state in ${}^6\text{Li}^{40}\text{K}$. The transition frequency from $|X^1\Sigma^+, v=0, J=0\rangle$ to $|b^3\Pi_0, v'=0, J'=1\rangle$ is determined to be 314,230.5(5)GHz. Assisted by microwave spectroscopy, we resolved the rotational structure of $|b^3\Pi_0, v'=0\rangle$ and extracted a rotational constant of $h \times 8.576(44)$ GHz for the $b^3\Pi_0$ state. From this, we deducted an energy separation between $|b^3\Pi_0, v'=0, J'=0\rangle$ and $|X^1\Sigma^+, v=0, J=0\rangle$ of $hc \times 10,481.03(2)$ cm⁻¹. Our work provides timely and precise information on the deeply-bound region of the $b^3\Pi_0$ triplet excited potential of LiK, and benefits future applications of ultracold LiK isotopologues in quantum simulation and quantum computation that demand long coherence times.

I. INTRODUCTION

The vibrational ground state of the $b^3\Pi_0$ potential of ultracold bialkali molecules is perturbed by the $A^1\Sigma^+$ electronic potential due to spin-orbit coupling (SOC). Therefore, it weakly couples to the rovibrational ground state of the $X^1\Sigma^+$ potential via an electronic dipole transition[1]. This makes the $|b^3\Pi_0, v'=0\rangle$ excited state a good candidate for the investigation and control of these ultracold ground state molecules. A laser beam tuned near the transition frequency between the two molecular levels conveniently changes the polarizability of the rotational ground state and the first rotationally excited state of the $X^1\Sigma^+$ vibrational ground state, allowing for magic or tune-out conditions for the microwave transition between these two rotational states [2]. Long coherence times over 1 second for the microwave transition of the ground state molecules can be achieved in an external optical potential formed by such laser beams under magic conditions [3], allowing for exploring quantum many-body physics with longrange dipole-dipole interactions [4], studying SU(N) physics [5], and performing quantum information processing with ultracold polar molecules [6–8].

Systematic experimental studies of the $b^3\Pi_0$ potential for bialkali molecules and determination of the ground-state energy are limited to heavy molecules [2, 9, 10]. So far, the spectroscopic study of LiK molecules has focused on the excited singlet potentials [11–16], as they strongly couple to the singlet $X^1\Sigma^+$ ground state potential. To the best of our knowledge, there are no reported experimental study of deeply bound molecular states in the excited triplet potential of LiK.

Here, we report the first observation of the vibrational ground state of the $b^3\Pi_0$ potential for LiK molecules. We prepared a tunable diode laser system at 954 nm for probing the transition for achieving magic wavelength from $|X^1\Sigma^+, \nu=0, J=0\rangle$ to $|b^3\Pi_0, \nu'=0, J'=1\rangle$, where ν and J are the vibrational and rotational quantum numbers. The transition resonance is determined by measuring the population loss feature of ultracold ${}^6\text{Li}{}^{40}\text{K}$ molecules. The resonance frequency is determined to be 314.2305(5) THz.

II. ULTRACOLD ⁶Li⁴⁰K MOLECULES

A. Production of molecules

In each experiment, around 3,000-10,000 ⁶Li⁴⁰K molecules are produced in a crossed optical dipole trap inside an ultrahigh-vacuum quartz cell. Weakly-bound Feshbach molecules are created via magneto-association in an ultracold atomic mixture of 5×10^4 ⁶Li and 1×10^5 ⁴⁰K atoms by adiabatically ramping down the magnetic bias field across the Feshbach resonance at 21.56 mT [17, 18]. These molecules are subsequently transferred to the singlet rovibrational ground state $|X^1\Sigma^+, v=0, J=0\rangle$ via a singlet excited state $|A^1\Sigma^+, v'=23, J'=1\rangle$ by stimulated Raman adiabatic passage (STIRAP) with a single-trip efficiency of 96% [19, 20]. The relevant states are labeled in Fig. 1(a). The ground-state molecules are subsequently transferred back to the Feshbach state v = 47 for detection with the light used for atomic transition.

^{*} These authors contributed equally.

[†] Electronic address:phydk@nus.edu.sg

A Production of molecules 2

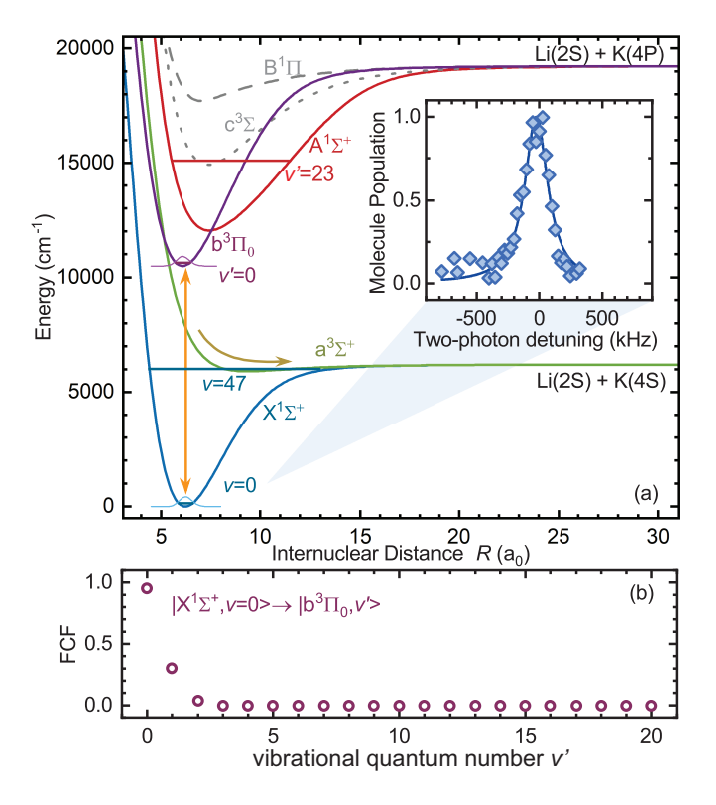


Figure 1. Potential Energy Curves for LiK [21]. (a) $X^1\Sigma^+$ (blue curve) and $a^3\Sigma^+$ (green curve) ground state potentials at large R connect to the Li(2S) plus K(4S) atomic asymptote. From the Li(2S)+K(4P) asymptote, four adiabatic potential curves are obtained. Two relevant potentials are the $A^1\Sigma^+$ (red curve) and $b^3\Pi_0$ (purple curve) potentials, which are coupled by spin-orbit interaction. The orange arrow indicates the transition from $|X^1\Sigma^+, v=0\rangle$ to $|b^3\Pi_0, v=0\rangle$. $|b^3\Pi_0, v=0\rangle$ can decay via a pre-dissociation process due to coupling to $a^3\Sigma^+$ as indicated by the curved arrow. The $B^1\Pi$ (gray dashed line) and $c^3\Sigma$ (gray dotted line) potentials are not considered in this work. Inset: Change in detected Feshbach molecules as a function of two-photon detuning (blue diamonds). A Lorentzian fit (blue curve) gives an full-width-half-maximum 2w of 224(13) kHz. (b) Calculated Franck-Condon factors (FCF) for transition from the singlet ground state to deeply-bound vibrational states in the $b^3\Pi$ excited potential (purple circles).

B. Potential energy curves

For the prediction of the ground state wavelength, we use the ab initio potentials by Allouche et al. [21]. As shown in Fig. 3 (a), the equilibrium position $R_0^b = 6.08 \, a_0$ of the $b^3\Pi$ potential matches well with $R_0^X = 6.24 \, a_0$ of the $X^1\Sigma^+$ potential. This leads to a vibrational wavefunction overlap integral of 0.95 between the vibrational ground states of the two potentials, i.e. the Franck-Condon factor (FCF) as shown in Fig. 1 (b). Other available ab initio LiK potentials have been summarized by Miadowicz et al. [22].

III. SPECTROSCOPY

A. Estimation of transition strength

Due to spin-orbit interaction, the lowest few bound states of the $b^3\Pi_0$ potential carry very weak spin-singlet character of $A^1\Sigma^+$. Therefore, the wavefunction of a $b^3\Pi_0$ ro-vobrational state $\left|\Psi^b_{\nu',J',m_{J'}}\right\rangle$ can be expressed as:

$$\left|\Psi^{\mathbf{b}}_{\mathbf{v}',J',m_{J'}}\right\rangle = \left(c_{1}\left|\mathbf{A}^{1}\Sigma^{+}\right\rangle + c_{2}\left|\mathbf{b}^{3}\Pi_{0}\right\rangle\right) \otimes \left|\psi^{\mathbf{b}}_{\mathbf{v}'}\right\rangle \otimes \left|\Phi_{J',m_{J'}}\right\rangle. \tag{1}$$

Here, c_1 and c_2 are the projection amplitudes of the electronic wavefunction on the adiabatic states $A^1\Sigma^+$ and $b^1\Pi_0$, which are calculated by diagonalizing the spin-orbit interaction Hamiltonian plus the energies of the adiabatic states as shown in Fig. 2 (a) & (b). c_1 is estimated to be 0.0062 for $|b^3\Pi_0,v'=0\rangle$ using $R_0^b=6.08\,e_{\,a_0}$, as the ground state wavefunction is gaussian-like. This factor strongly depends on the position where the A and b potential curves crosses and on the magnitude of the SOC elements, and is therefore subject to an error range of up to ± 1 order of magnitude. The second and third terms are the vibrational and rotational wavefunctions. The transition from $|X^1\Sigma^+,v=0,J=0\rangle$ to $|b^3\Pi,v'=0,J'=1\rangle$ is therefore an electronic dipole transition, and the corresponding transition dipole matrix element for laser polarization p can be calculated by

The angular momentum dependence is described in the second line of the equation by the geometrical factors. The second term on the third line represents the transition dipole moment (TDM) evaluated at the Condon point $R_{\rm C}$. We adopt the ab initio results published in our previous work [19] and replotted in Fig. 2 (c). At $R_{\rm C}=6.17~a_0$ as shown in Fig. 2 (d), we estimate a TDM of 3.75 $e\,a_0$. Therefore, the transition dipole matrix element $\langle\hat{a}\rangle$ is estimated to be $2.6\times10^{-2}~e\,a_0$, corresponding to a partial linewidth of $\Gamma/2\pi=263~{\rm Hz}$.

B. Prediction of resonance frequency

The wavelength of the transition is estimated by calculating the energies of the $|X^1\Sigma^+, \nu=0, J=0\rangle$ and $|b^3\Pi, \nu'=0, J'=1\rangle$ states, which are obtained by solving the Schrödinger equation with the ab initio potentials using the Fourier-grid Hamiltonian method [25]. With the ab initio potential curves [21] as shown Fig. 1 (a), the transition wavenumber is calculated to be $10,490\,\mathrm{cm}^{-1}$. The largest uncertainty in the calculation is from the term energy T_e (referenced to the bottom of $X^1\Sigma^+$) of the $b^3\Pi_0$ potential, which

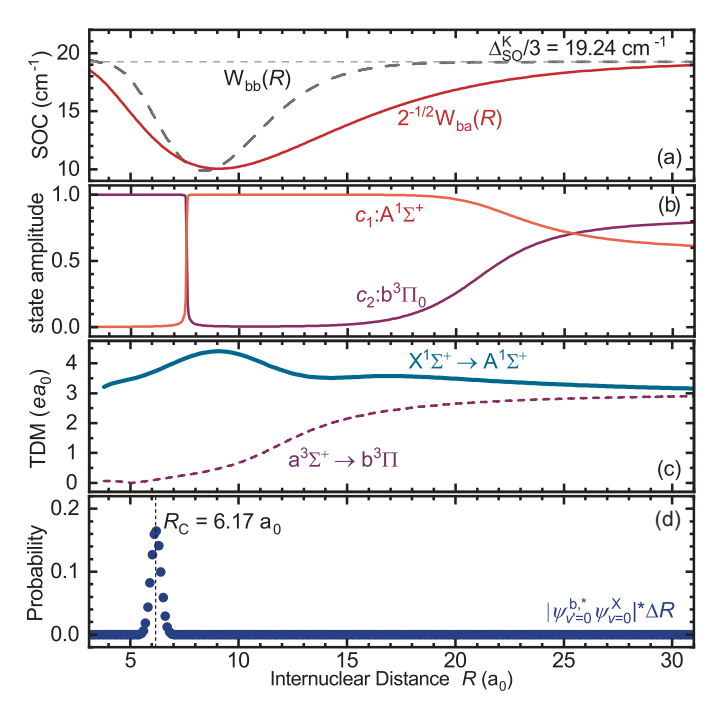


Figure 2. **Calculations for SOC and FCFs.** (a) $W_{bb}(R)$ (dashed line) and $W_{ba}(R)$ (red solid line) are the R dependent diagonal and off-diagonal elements of the A-b SOC matrix. (b) State projection amplitudes on the adiabatic basis for $A^1\Sigma^+$ (red curve) and $b^3\Pi_0$ (purple curve). (c) Transition dipole moments [19] for $X^1\Sigma^+ \to A^1\Sigma^+$ (blue curve) and $a^3\Sigma \to b^3\Pi$ (purple dashed curve). (d) Overlapping probability distribution (purple circles) for transitions from $|X^1\Sigma^+, \nu=0\rangle$ to $|b^3\Pi_0, \nu'=0\rangle$ sampled at a grid size of ΔR . The vertical short dashed line indicates the Condon point R_C at 6.17 ea_0 .

is typically around 1% for ab initio calculations. This corresponds to an uncertainty of 105 cm⁻¹ (or approximately 3 THz) for $|b^3\Pi_0, v'=0, J'=1\rangle$. In our experiment, the cycle time for taking one data point is approximately 3 min. Therefore a better prediction for the transition frequency is necessary to reduce the experimental effort for the spectroscopic search. In the Supplement Information of the work by A. Grochola et al. [15] multiple perturbed spectral lines in the deeply bound region of the $A^1\Sigma^+$ potential are included. These perturbations can only be caused by ro-vibrational states of the $b^{3}\Pi_{0}$ potential. In their work [15] these lines were discarded without further systematic analysis. However, we found that these perturbed lines may provide indications for locating the $|b^3\Pi_0, v'=0\rangle$. In Fig. 3, the rotational energies for some of the deeply-bound vibrational states of $A^1\Sigma^+$ measured by Grochola et. al. [15] with clear signals of perturbation are plotted. While most of the measured transition lines can be described by a Dunham expansion [26], some lines show clear signals of perturbation. This applies for lines with an energy deviation of $\Delta E > 0.1 \, \mathrm{cm}^{-1}$ from the Dunham fit of the A¹ Σ^+ potential. The energy of a rovibrational state in a certain adiabatic electronic potential can be expressed using the Dunham series as

$$E(v, J, \Omega) = \sum_{k,l} Y_{k,l} (v + \frac{1}{2})^k [J(J+1) - \Omega^2]^l.$$
 (2)

 $Y_{k,l}$ quantities are Dunham coefficients related to the shape of electronic potentials[26], which can be precisely determined by fitting the spectroscopic data with Eqn. 2. For rovibrational states in the $A^1\Sigma^+$ and $b^3\Pi_0$ potentials the quantum number Ω for the projection of the total electronic angular momentum on the internuclear axis is zero. The energy of rotational levels J' for several vibrational states v' of the $A^1\Sigma^+$ potential, which are referenced against $|X^1\Sigma^+, v=0, J=J'-1\rangle$, are plotted using the experimentally determined Dunham coefficients [15, 23] as shown with the green curves in the upper panels of Fig. 3.

For each perturbed feature in Fig. 3(a)-(f), a data point with low residual shift ΔE is selected, which we interpret to represent the center of the crossing. We use the J' value of the selected point as assigned by Grochola et al.[15] to represent the center of perturbation. The selection rule for the perturbation of the rotational states due to spin-orbit coupling is $\Delta J = 0$ [27]. The curves describing the rotational energy progression of vibrational states in $b^3\Pi_0$ potential should cross the curves for the vibrational levels of $A^1\Sigma^+$ potential at the rotational quantum number J's indicating the center of the perturbed regions. To calculate the energies for deeply-bound rovibrational states of the $b^3\Pi_0$ potential we use the ab initio potential as shown in Fig. 1. The $b^3\Pi_0$ potential curve is truncated to retain the lower half of the potential well, corresponding to energies below half of the potential depth $\mathcal{D}_e/2$. It is then re-parameterized by modifying the internuclear distance $R \rightarrow x = (R - R_e)/R_e$, where R_e is the equilibrium distance of the potential. The deeply-bound region of the curve is fitted with a polynomial function $f(x) = T_e + \sum_{i=2}^{10} \alpha_i x^i$, where T_e is the energy offset for the potential bottom. The Dunham coefficients $Y_{k,l}$ of $b^3\Pi_0$ can be expressed by combinations of the fitted parameters α_i and the equilibrium rotational constant $B_e = h/(c8\pi^2\mu R_e^2)$ [26]. μ is the reduced mass of ⁷Li³⁹K isotopologue. The above process is repeated for the ab initio $X^1\Sigma^+$ potential curve for extracting the Dunham coefficients. The calculated energies of $|b^3\Pi_0, v', J'\rangle$ using the fitted Dunham coefficients, which are referenced against $|X^1\Sigma^+, v=0, J=J'-1\rangle$, are shown by the blue curves in the upper panels of Fig. 3. As a second step to achieve crossings in the perturbation region we shift T_e and hence shifting energies of the rovibrational states of $b^3\Pi_0$ simultaneously. At a shift of -8 cm⁻¹, good agreement is found between the rotational quantum number J', at which the two curves intersect, and the center of the perturbation. This is quantitatively supported by minimizing the sum, over all six subfigures, of the squared error between the $A^1\Sigma^+$ - $b^3\Pi_0$ rovibrational energy differences at J' and a variable energy offset. This means that the minimum of the ab-initio adiabatic potential for $b^3\Pi_0$ is approximately 8 cm^{-1} too high, independent of the choice of isotopologue. In the following we apply the shift to all predicted lines for ⁶Li⁴⁰K isotopologue and obtain a transition wavenumber for $|X^1\Sigma^+, v=0, J=0\rangle \rightarrow$ $|b^{3}\Pi_{0}, v' = 0, J' = 1\rangle$ of 10,481.9 cm⁻¹, which corresponds to the laser frequency of 314,239 GHz. Here, we give a conservative uncertainty range of $\pm 5\,\mathrm{cm}^{-1}$ for the prediction of the v'=0 state. Apart from T_e , deviations in the potential shape will also affect the prediction for the transition frequenC Laser Setup 4

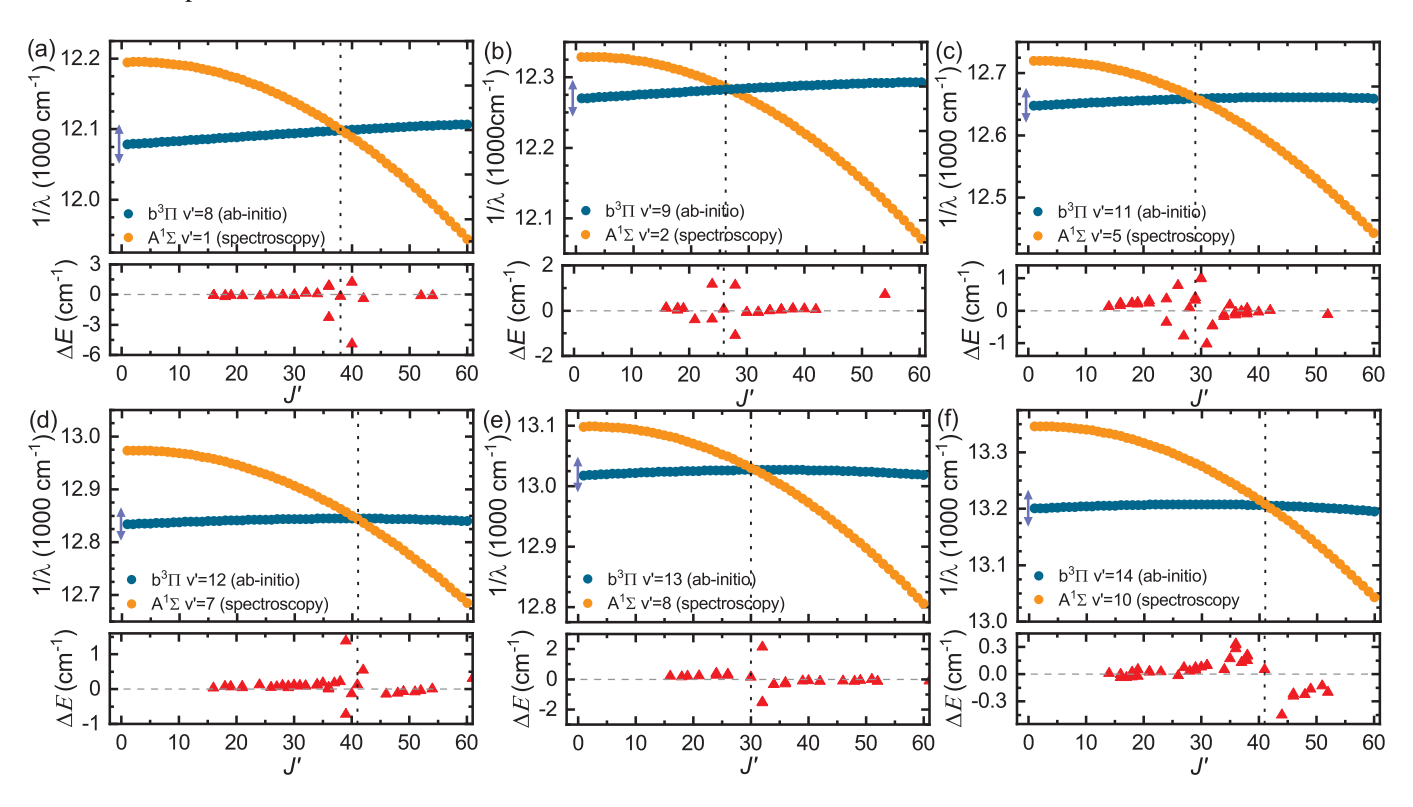


Figure 3. (a) - (f): Upper panels show the rotational energy progression of a vibrational state of the $A^1\Sigma^+$ potential (orange circles) calculated using spectroscopically determined Dunham coefficients [15, 23] together with the rotational energies of a vibrational level in the $b^3\Pi_0$ potential (blue circles), which is calculated by using Dunham coefficients based on ab initio potentials [21]. Both $A^1\Sigma^+$ and $b^3\Pi_0$ transitions are derived from the same ground state $X^1\Sigma^+|\nu=0,J=J'-1\rangle$. Lower panels show the error ΔE (red triangles) between experimentally observed transition energies for $A^1\Sigma^+$ potential and transitions calculated using Dunham coefficients reported by Grochola et al. [15]. Observed transitions with ΔE higher than 0.1cm⁻¹ are considered as perturbation caused by $b^3\Pi_0$ rovibrational levels. The vertical dashed lines indicate the center for the perturbation region, which is studied more thoroughly for other heavier species [24].

cies. However, the uncertainty due to the leading Dunham term ω_e , which describes the harmonic vibration frequency of the potential, is expected to be only $1\,\mathrm{cm}^{-1}$ assuming a 1% error for the ab initio calculations. Its contribution to the total uncertainty in the energy of $|b^3\Pi_0, v=0, J=1\rangle$ is therefore almost negligible. Based on the above empirical analysis the uncertainty is now significantly reduced from approximately 3 THz to 300 GHz, corresponding to $\pm 5\,\mathrm{cm}^{-1}$. Indeed, as will be shown later in Sec. III D, the transition was found within the interval.

C. Laser Setup

For achieving high laser power and frequency tunability, we built an external-cavity diode laser and use it to seed a tapered amplifier for power amplification. The laser diode has an anti-reflection coating to allow for wavelength tuning from 940 nm to 980 nm. The free-running short-term linewidth of the ECDL is around 2 MHz. The TA is seeded with approximately 20 mW laser power and provides an output power up to 700 mW. In the experiment, the wavelength of the laser is monitored by a wavemeter (WS-7, High Finesse) and adjusted in 500 MHz steps when searching for the resonance. In the experiment, we focused around 500 mW of laser

power on the molecules to a $1/e^2$ Gaussian-beam waist of 80 μ m, which allows for an estimated laser Rabi frequency of $\Omega = 2\pi \times 65$ MHz.

D. Measurement

In each measurement, ⁶Li-⁴⁰K Feshbach molecules are first transferred to the ground state $|X^1\Sigma^+, v=0, J=0\rangle$ and transferred back to the Feshbach state using STIRAP for detection. During this process, the spectroscopy beam at 954nm is switched on to introduce an AC Stark shift. When the spectroscopy laser scans in the far-off-resonant range, the threelevel STIRAP system experiences an almost constant energy shift, which is considered as a fixed background and compensated by shifting the frequency of the STIRAP lasers. The half-width at half-maximum (HWHM) of the STIRAP twophoton line profile is measured to be 112(10) kHz. For the given laser intensity and transition strength estimated in Section III A, we will only be able to observe significant molecular number losses when the spectroscopy laser is within a range of ± 10 GHz. The losses are induced by the AC Stark shift of the STIRAP two-photon resonance for equal or larger than one HWHM. As the uncertainty in $\langle \hat{d} \rangle$ is dominated by c_1 , which may be overestimated by up to one order of magniD Measurement 5

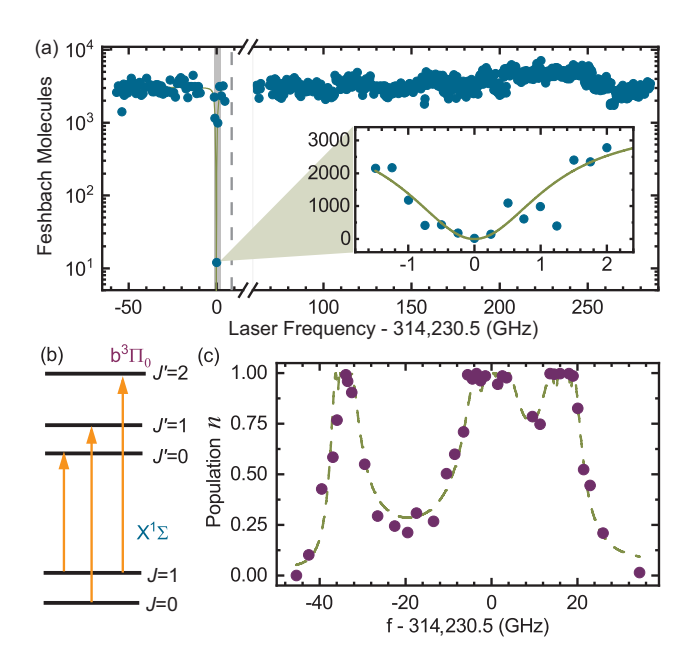


Figure 4. **Spectroscopy measurement for** $b^3\Pi_0$. (a) The number of Feshbach molecules is recorded (blue circles) while scanning the frequency of spectroscopy laser. Green curves are fit to the data. (b) Illustration of rotational level scheme for the ground state and target excited state. (c) Population of molecules is recorded after a microwave π pulse (purple circles), which drives the transition $|J=0,m_j=0\rangle \rightarrow |J=1,m_j=-1\rangle$. The spectroscopy laser is switched on during the process. The three peaks are caused by the $|J=0\rangle \rightarrow |J'=1\rangle$, $|J=1\rangle \rightarrow |J'=0,2\rangle$ transitions. Green dashed curves are fit to the data.

tude, the scanning step of the laser frequency is chosen to be 1 GHz to avoid missing the transition. The measured molecular loss spectrum for a frequency range from 314,173.5 GHz to 314,516.0 GHz is shown below in Fig. 4 (a). A narrow resonance is found to be centered at 314,230.5(5) GHz. The uncertainty in the determination of line center is limited by 0.5 GHz due to the instability of our spectroscopy laser. As the bottom of $b^3\Pi_0$ potential is much deeper than any other excited-state potentials by more than 30 THz, the measured transition resonance can only be explained by the transition from $|X^1\Sigma^+, v = 0, J = 0\rangle$ to $|b^3\Pi_0, v' = 0, J' = 1\rangle$. A scan with finer steps around the transition resonance is shown in the inset of Fig. 4 (a). The loss feature is modeled by a Lorentzian distribution $w^2/\pi(\delta(x,\Omega)^2+w^2)$ with $\delta(x,\Omega)$ being the AC Stark shift as a function of laser detuning x and the Rabi frequency Ω . w is the HWHM of the STIRAP twophoton linewidth. By fitting the decay curves, we extract a Rabi frequency of $\Omega = 2\pi \times 24(1)$ MHz. This indicates a much smaller $\langle \hat{d} \rangle$ of $9.6 \times 10^{-3} e \, a_0$.

Further, we probe the rotational structure of the excited state and locate the energy for the rovibrational ground state of $b^3\Pi$ potential. We use a microwave (MW) signal at 17.482 GHz to drive the Rabi oscillation between the ground state J=0 and the first excited state J=1 of the $\left|X^1\Sigma^+, \nu=0\right\rangle$ for a duration of 400 μ s, corresponding to half of a period (or π pulse). The spectroscopy laser is switched on for a du-

ration that covers the MW pulse. When the laser frequency is far off-resonance from the optical transitions to the rotational manifold of the $|b^3\Pi, v'=0\rangle$ as illustrated in Fig. 4 (b), the induced AC Stark shift can be treated as a fixed background and is compensated by shifting the MW frequency. While scanning laser frequency, the residual population n in $|X^1\Sigma^+, v=0, J=0\rangle$ is recorded after each MW- π pulse and the result is shown in Fig. 4 (c). At large laser detunings, the MW pulse drives the resonant Rabi π -pulse and transfers the full population to $|X^1\Sigma^+, v=0, J=1\rangle$, leading to depletion of n. Three peaks are observed while scanning the laser frequency close to the three transitions $J = 0 \rightarrow J' = 1 \& J = 1 \Leftrightarrow J' = 1 \& J = 1 \& J = 1 \Leftrightarrow J' = 1 \& J = 1 \Leftrightarrow J$ J' = 0,2, which locate at the detunings of $h\Delta = 0, -2B_0^{\rm X}$ $2B_0^b$, and $4B_0^b - 2B_0^X$. B_0^X and B_0^b are the rotational constants for $X^{1}\Sigma^{+}$ & $b^{3}\Pi_{0}$ vibrational ground states. The increase in population at these laser detunings can be modeled by a Rabi oscillation processes at a detuning due to laser-induced AC Stark shift, which is contributed by the sum of the three transitions. $B_0^X/h = 8.742(3)$ GHz was previously determined experimentally [19]. By fitting the data using the model described above, we obtained $B_0^{\rm b}/h = 8.576(44)$ GHz. Here, we do not consider the effect of the centrifugal distortion D_e on the position of the resonances. From the Dunham coefficients calculated using the ab initio curves we obtain a D_e/h of 73.5 kHz, which is four orders of magnitude smaller than the data resolution. The obtained rotational constant B_0^b is 9% smaller than our calculated value based on the equilibrium distance R_e 6.086 a₀ of the ab initio potential[21]. Moreover, the energy of $|b^3\Pi_0, v'=0, J'=0\rangle$ relative to $|X^1\Sigma^+, v=0, J=0\rangle$ is determined to be $E_0^b = h \times 314,213.3(5)$ GHz, corresponding to the wavenumber of $10,481.03(2) \text{ cm}^{-1}$. As the binding energy for $|X^1\Sigma^+, v=0, J=0\rangle$ has been precisely measured by our group using two-photon spectroscopy to be 6,104.18081(1) cm⁻¹ [19], the binding energy for $|b^3\Pi_0, v'=0, J'=0\rangle$ is determined to be 8,666.05(2) cm⁻¹ relative to the ⁴⁰K D2 asymptote.

IV. CONCLUSION

As a first step toward achieving magic conditions for the rotational coherence of ultracold ⁶Li⁴⁰K ground state molecules, we performed molecular spectroscopy to search for the weak transition from the absolute ground state of $X^1\Sigma^+$ potential to the vibrational ground state of $b^3\Pi_0$ excited state potential. The prediction for the transition frequency is assisted by analyzing the available spectroscopy data on perturbed transitions of deeply bound state in the $A^1\Sigma^+$ potential [15]. We first determined the transition frequency to be 314,230.5(5) GHz. By using a microwave field to couple the rotational ground and first excited state J=0,1 of $|X^1\Sigma^+,v=0\rangle$, we spectroscopically resolved the rotational structure (J' = 0, 1, 2)of the $|b^3\Pi_0, v'=0\rangle$ and extracted the rotational constant $B_0 = h \times 8.576(44)$ GHz. By replacing the diode laser setup with a high-power fiber-laser system frequency stabilized to an ultra-stable high-finesse cavity, we can achieve optical lattices operating at magic conditions to obtain long coherence times for ultracold ⁶Li⁴⁰K molecules interacting via strong dipole-dipole interactions. Our work also benefits the study of fermionic LiK isotopologues in their applications in quantum simulation and quantum computation in optical tweezer arrays.

AUTHOR CONTRIBUTIONS

A.Y. conceived the idea, provided predictions/corrections for the transition frequency, participated in the measurement, found the transition and wrote the manuscript; X.N. built the laser setup, predicted the transition strengths, conducted the measurement and found the transition; H.L.Y., Y.L., V.A. and C.H. participated in the measurement; J.K and S.K. conducted calculations for the SOC coupling, provided theoretical guidance; K.D. is the supervisor of this experimental work and provided guidance to the team; All authors have reviewed the manuscript.

CONFLICTS OF INTEREST

There are no conflicts to declare.

DATA AVAILABILITY

Data supporting this article, including the calculations of Franck-Condon factors, spin-orbit coupling strengths, predicted rovibrational transition frequencies, and spectroscopy measurements are available on Zenodo at https://doi.org/10.5281/zenodo.17386208.

ACKNOWLEDGEMENTS

The authors would like to thank Sofia Botsi and Sunil Kumar for their earlier contributions in the lab. This research is supported by the National Research Foundation, Singapore and A*STAR under its CQT Bridging Grant.

- [1] R. Vexiau, D. Borsalino, M. Lepers, A. Orbán, M. Aymar, O. Dulieu, and N. B. Maafa, International Reviews in Physical Chemistry 36, 709 (2017), https://doi.org/10.1080/0144235X.2017.1351821.
- [2] R. Bause, M. Li, A. Schindewolf, X.-Y. Chen, M. Duda, S. Kotochigova, I. Bloch, and X.-Y. Luo, Phys. Rev. Lett. 125, 023201 (2020).
- [3] P. D. Gregory, L. M. Fernley, A. L. Tao, S. L. Bromley, J. Stepp, Z. Zhang, S. Kotochigova, K. R. Hazzard, and S. L. Cornish, Nature Physics, 1 (2024).
- [4] A. N. Carroll, H. Hirzler, C. Miller, D. Wellnitz, S. R. Muleady, J. Lin, K. P. Zamarski, R. R. W. Wang, J. L. Bohn, A. M. Rey, and J. Ye, Science 388, 381 (2025).
- [5] B. Mukherjee, J. M. Hutson, and K. R. A. Hazzard, New Journal of Physics 27, 013013 (2025).
- [6] D. K. Ruttley, A. Guttridge, T. R. Hepworth, and S. L. Cornish, PRX Ouantum 5, 020333 (2024).
- [7] D. K. Ruttley, T. R. Hepworth, A. Guttridge, and S. L. Cornish, Nature 637, 827 (2025), published online 2024; in print 2025.
- [8] L. R. B. Picard, A. J. Park, G. E. Patenotte, S. Gebretsadkan, D. Wellnitz, A. M. Rey, and K.-K. Ni, Nature 637, 821 (2025), published online 13 November 2024; in print 2025.
- [9] J. Kobayashi, K. Aikawa, K. Oasa, and S. Inouye, Phys. Rev. A 89, 021401 (2014).
- [10] H. Harker, P. Crozet, A. J. Ross, K. Richter, J. Jones, C. Faust, J. Huennekens, A. V. Stolyarov, H. Salami, and T. Bergeman, Phys. Rev. A 92, 012506 (2015).
- [11] V. Bednarska, A. Ekers, P. Kowalczyk, and W. Jastrzebski, The Journal of Chemical Physics 106, 6332 (1997), https://pubs.aip.org/aip/jcp/article-pdf/106/15/6332/19166361/6332_[24] A. Grochola, J. Szczepkowski, W. Jastrzębski, and P. Kowal-1_online.pdf.
- [12] A. Pashov, W. Jastrzębski, and P. Kowalczyk, Chem. Phys. Lett **292**, 615 (1998).

- [13] S. Rousseau, A. Allouche, M. Aubert-Frécon, S. Magnier, P. Kowalczyk, and W. Jastrzebski, Chem. Phys. 247, 193 (1999).
- [14] A. Ridinger, S. Chaudhuri, T. Salez, U. Eismann, D. Fernandes, K. Magalhães, D. Wilkowski, C. Salomon, and F. Chevy, Eur. Phys. J. D **65**, 223 (2011).
- [15] A. Grochola, J. Szczepkowski, W. Jastrzebski, and P. Kowalczyk, Chemical Physics Letters 535, 17 (2012).
- [16] S. Botsi, A. Yang, M. M. Lam, S. B. Pal, S. Kumar, M. Debatin, and K. Dieckmann, Physical Chemistry Chemical Physics 24, 3933 (2022).
- [17] E. Wille, F. M. Spiegelhalder, G. Kerner, D. Naik, A. Trenkwalder, G. Hendl, F. Schreck, R. Grimm, T. G. Tiecke, J. T. M. Walraven, S. J. J. M. F. Kokkelmans, E. Tiesinga, and P. S. Julienne, Phys. Rev. Lett. 100, 053201 (2008).
- [18] T. G. Tiecke, M. R. Goosen, J. T. M. Walraven, and S. J. J. M. F. Kokkelmans, Phys. Rev. A 82, 042712 (2010).
- [19] A. Yang, S. Botsi, S. Kumar, S. B. Pal, M. M. Lam, I. Čepaitė, A. Laugharn, and K. Dieckmann, Phys. Rev. Lett. 124, 133203
- [20] C. He, X. Nie, V. Avalos, S. Botsi, S. Kumar, A. Yang, and K. Dieckmann, Phys. Rev. Lett. 132, 243401 (2024).
- Allouche, Website of A.R. https://sites.google.com/site/allouchear/Home/diatomic.
- [22] Ł. Miądowicz, P. Jasik, and J. E. Sienkiewicz, Central European Journal of Physics **11**, 1115 (2013).
- [23] E. Tiemann, H. Knöckel, P. Kowalczyk, W. Jastrzebski, A. Pashov, H. Salami, and A. J. Ross, Phys. Rev. A 79, 042716
- czyk, Journal of Quantitative Spectroscopy & Radiative Transfer 145, 147 (2014).

- [25] C. C. Marston and G. G. Balint-Kurti, The Journal of Chemical Physics **91**, 3571 (1989).
- [26] J. L. Dunham, Phys. Rev. 41, 721 (1932).

[27] H. Lefebvre-Brion and R. W. Field, *The Spectra and Dynamics of Diatomic Molecules: Revised and Enlarged Edition* (Academic Press (Elsevier), Amsterdam, 2004).